A-D-A structured phototheranostics for NIR fluorescence imaging guided Type I/II photodynamic and photothermal therapy of tumor

Xinyu Wang[a,#], Houxian He[b,#], Yunquan Yang[a], Shaojing Zhao[c], Yuanyu Tang[c], E Pang[c], Qingxu Diao[d], Mingqin Xiong[a], Jianing Yi[d], Minhuan Lan[c,*], Dayong Xu[a,b,*]

[a]Department of General Surgery, The Affiliated Changsha Hospital of Xiangya School of Medicine, Central South University, Changsha, 410005, China

[b]Graduate Collaborative Training Base of The first hospital of Changsha, Hengyang Medical School, University of South China,Hengyang, Hunan,421001,China

[c]College of Chemistry and Chemical Engineering, Central South University, Changsha, 410083, China

[d]Department of Breast and Thyroid Gland Surgery, Hunan Provincial People's Hospital, The First Affiliated Hospital of Hunan Normal University, Changsha, 410005, China

Xinyu Wang and Houxian He Contributed equally to this work.

*Corresponding Authors:

Dayong Xu: xdycs@qq.com; Minhuan Lan: minhuanlan@csu.edu.cn

Materials

The following materials were used in this study: 4TIC was acquired from Organtec Co., Ltd., DSPE-PEG-NH_2-2000 was sourced from Shanghai ToYong Bio-

Technology Co., Ltd., Wuhan Saiye Biotechnology Co., Ltd provided the MC38 cell line. Six-week-old female C57BL/6 mice were acquired from Hunan SJA Laboratory Animal Co., Ltd.

Instruments

Ultraviolet-visible (UV-Vis) spectra were recorded using a Shimadzu UV-2600 spectrophotometer. Fluorescence spectra were measured with an RF-6000 spectrofluorophotometer. Scanning electron microscopy (SEM) images were acquired using a JSM-7610FPlus microscope (JEOL Ltd.). Fluorescence images of cells were captured using a Leica DMIL LED inverted fluorescence microscope and confocal laser scanning microscope (CLSM, Leica SP8). The 808 nm laser was was obtained from Shanghai Xilong Optoelectronics Technology Co., Ltd. (Shanghai, China).

Theoretical calculations

All theoretical calculations were performed using Gaussian 16, Revision C.01 (Gaussian, Inc., Wallingford, CT, 2019). For density-functional theory (DFT) calculations, the HOMO/LUMO orbitals of the monomer and the ground-state (S_0) molecular geometries were optimized at the B3LYP/6-31G(d) level. The electrostatic potential was then calculated based on the optimized S_0 molecular geometries at the same level and analyzed using Multiwfn 3.8 dev. The HOMO/LUMO orbitals of the dimer were optimized using the B3LYP-GD3BJ/6-31G(d) method. For time-dependent DFT (TD-DFT) calculations, molecular geometry optimization was carried out in the first singlet excited state (S_1), and the excited energies and excitation state transitions (EST) were calculated using the B3LYP functional with the 6-31G(d) basis

set. The HOMO/LUMO orbitals surface maps were visualized using the Visual Molecular Dynamics (VMD) program.

Preparation of 4TIC NPs

A solution was prepared by dissolving 2.8 mg of 4TIC and 5.5 mg of DSPE-PEG-NH_2-2000 in 1.0 mL of tetrahydrofuran (THF), which was then gradually introduced drop by drop into 20.0 mL of water while being ultrasonically agitated. The solution was transferred to a dialysis bag (MWCO = 3500 DA) and dialyzed with magnetic stirring for 24 h, changing the water every 4 h to remove excess DSPE-PEG-NH_2 and THF.The resulting aqueous solution of 4TIC nanoparticles was kept at 4°C in the dark.

Determination of $^1O_2$ in 4TIC NPs solution

1 μL of Singlet Oxygen Sensor Green (SOSG) was mixed with 2.0 mL of an 4TIC nanoparticle solution at a concentration of 5 μM. The solution was then subjected to irradiation using a 808 nm laser at a power density of 0.1 W/cm², and the fluorescence spectra of SOSG were captured every 5 seconds. To compare, the fluorescence spectra of SOSG in pure water were recorded under identical conditions.

Determination of superoxide anion ($O2^{-\cdot}$) in 4TIC NPs solution

5 μL DHR 123 solution was added to 2.0 mL 4TIC NPs solution (5 μM). The solution was irradiated with a 808 nm laser (0.5 W/cm²). The fluorescence spectra of DHR 123 were recorded every 30 seconds. For comparison, the fluorescence spectrum of DHR 123 in pure water was also measured under the same conditions.

Examination of the photostability of 4TIC NPs solution

The 4TIC nanoparticle solution at a concentration of 5.0 μM was exposed to a 808 nm laser with a power density of 0.5 W/cm² for a duration of 10 min, with absorption spectra recorded every 2 min. For comparison, the absorption spectra of indocyanine green (ICG) (5.0 μM) were assessed under identical conditions.

Evaluation of the stability of 4TIC NPs solution

The 4TIC NPs solution, with a concentration of 5.0 μM, was kept at 4°C away from light. Its absorption spectrum and particle size distribution were checked daily over a week.

Assessment of temperature shifts in 4TIC NPs solution

4TIC NPs solutions with concentrations of 0, 2.5, 5, 10, and 20 μM underwent irradiation using a 808 nm laser at a power density of 1 W/cm² for a duration of 10 min. A thermocouple and an infrared thermal imaging camera were used to measure the temperature change of the solution throughout the irradiation process.

Examination of the photothermal cycle in solutions of 4TIC NPs

1.0 mL of 4TIC nanoparticle solution (5 μM) was irradiated with a 808 nm laser at a power density of 1 W/cm² for 10 minutes. After allowing the solution to cool to room temperature, a second 10-minute irradiation was performed. For comparison, the temperature change of a ICG solution (5 μM) was measured under the same conditions.

Evaluation of the photothermal conversion efficiency of 4TIC NPs

The absorbance of the 4TIC nanoparticle solution at 808 nm was adjusted to approximately 0.2. It was then exposed to a 808 nm laser with a power density of 1

W/cm² for 10 min, followed by a cooling phase of 10 min. Under the same conditions, the temperature shift of pure water was also measured for comparison, and η can be evaluated using the following two equations.

$$\eta = \frac{hA \triangle T_{max} - Q_{dis}}{I\,(1-10^{-A_\lambda})}$$

$$\tau = \frac{m_D c_D}{hA}$$

Wherein, $\triangle T_{max}$ is defined as the maximum temperature difference achieved at the steady state. For 4TIC, this value is 17.5°C. Q_{dis} is the heat dissipation of water, and it can be calculated to be 0.03399. I denotes the power density of the 808 nm laser, which is 1 W/cm², and A_λ is the absorbance of 4TIC at 808 nm, recorded as 0.212. m_D is the mass of water, which is 1 g; c_D is the specific heat capacity of water, which is 4.2 J/gK; and τ is the time constant for heat transfer, determined to be 458.948 s. According to this formula, hA is calculated to be 0.16015 W/K. Therefore, the value of η can be calculated to be 32.7%.

Cell culture

The MC38 cells, a mouse colon carcinoma cell line, were cultured in RPMI 1640 medium supplemented with 10% fetal bovine serum. They were kept in a humidified incubator at 37°C with 5 % CO_2. When necessary, the cells were treated with a 0.25 % trypsin-EDTA solution and passaged for further use.

Cellular Uptake Mechanism Study

To investigate the endocytic pathways of 4TIC NPs, MC38 cells were pre-treated with various pharmacological inhibitors for 1 h prior to the addition of NPs. The inhibitors and their concentrations were as follows: 10 μM chlorpromazine (an

inhibitor of clathrin-mediated endocytosis), 1 μg/ml Methyl-β-cyclodextrin (an inhibitor of caveolae-mediated endocytosis), 50 μM amiloride (an inhibitor of macropinocytosis), and incubation at 4 °C for 12 hours to inhibit all energy-dependent endocytosis. After pre-treatment, the cells were incubated with 4TIC NPs (20 μM) for 4 h in the continued presence of the inhibitors. The cells were then thoroughly washed with PBS. Fluorescence images were acquired using an inverted fluorescence microscope, and cellular uptake efficiency was quantified by flow cytometry. Cells without inhibitor treatment were used as the control.

Subcellular Localization Analysis

The intracellular distribution of 4TIC NPs was determined by confocal laser scanning microscopy (CLSM) using organelle-specific trackers. MC38 cells were incubated with 20 μM 4TIC NPs for 4 h. Subsequently, the cells were co-stained with 100 nM MitoTracker and 75 nM LysoTracker for 30 min at 37°C according to the manufacturer's instructions. Fluorescence images were captured using a confocal laser scanning microscope.

Cytotoxicity assay

Cytotoxicity Assay: The MTT assay was used to assess the cytotoxicity of 4TIC NPs toward MC38 cells. A total of 2×10^4 cells per well were placed into 96-well plates and left to incubate for 24 h. Following incubation, the cells were subjected to different concentrations of 4TIC NPs without light for 20 h. Next, 200 μL of RPMI 1640 medium with 0.5% MTT was introduced to each well, and the plate was incubated for another 4 h. The medium was then removed, and 150 μL of dimethyl

sulfoxide (DMSO) was added to each well, followed by gentle shaking. The absorbance was subsequently recorded at 490 nm with a microplate reader.

Phototoxicity Assay: To evaluate phototoxicity, cells were exposed to 4TIC nanoparticles in darkness for 4 h, followed by irradiation with a 808 nm laser at a power density of 1 W/cm² for 10 min. Afterward, the cells were incubated for a further 16 h. The subsequent steps were the same as those outlined for the cytotoxicity assay.

To achieve individual PDT and PTT treatments, we maintained a constant temperature (25℃) or treated the cells with 100 μM ascorbic acid. The remaining steps were the same as those described for the phototoxicity test.

Intracellular reactive oxygen species (ROS) test

The cells were divided into four groups: PBS, PBS + L, 4TIC NPs, and 4TIC NPs + L, where "L" denotes laser irradiation. To assess the production of ROS, different fluorescent probes were used: A green fluorescent probe, O22, for $^1O_2$ detection, and a red fluorescent probe, DHE, for intracellular $O2^{-\cdot}$ detection.

$^1O_2$ detection: MC38 cells were cultured in 24-well plates until they reached 60%-70% confluence. RPMI 1640 medium containing 20 μM 4TIC NPs was then added to the cells for co-culture for 4 h. The cells were incubated with an O22-diluted medium for 30 min. Cells in the PBS + L and 4TIC NPs + L groups were irradiated with a 808 nm laser (1 W/cm²) for 10 min. Images were taken using a fluorescent inverted microscope.

$O2^{-\cdot}$ detection: MC38 cells were cultured in 24-well plates until they reached 60%-70% confluence. RPMI 1640 medium containing 20 μM 4TIC NPs were co-cultured

with the cells for 4 h. The cells were incubated with a DHE-diluted medium for 30 min. Cells in PBS + L and 4TIC NPs + L groups were irradiated with a 808 nm laser (1 W/cm^2) for 10 min. Images were taken using a fluorescent inverted microscope.

Mitochondrial membrane potential (MMP) detection

MC38 cells were placed in 24-well plates and grown until they reached 60-70% confluence. Subsequently, the cells received treatment with RPMI 1640 medium that contained 20 μM 4TIC nanoparticles for 4 h, while the PBS group was used as the control. In the laser-treated groups (PBS + L and 4TIC NPs + L), cells were exposed to a 808 nm laser at a power density of 1 W/cm^2 for a duration of 10 min. Following treatment, the cells were carefully rinsed twice with pre-heated PBS and kept at 37 °C in darkness for 20 min with JC-1 staining solution (5 μg/mL in serum-free RPMI 1640). Following incubation, the staining solution was taken out, and the cells were rinsed two times with JC-1 washing buffer. Imaging was then performed. Mitochondrial membrane potential was evaluated by measuring red and green fluorescence using a fluorescence microscope.

Mitochondrial permeability transition pore (mPTP) detection

Following the same cell culture and treatment protocol as the JC-1 assay, cells were incubated without light at 37°C with RPMI 1640 medium containing 1 μM Calcein-AM and 1 mM $CoCl_2$ for 30 min. $CoCl_2$ was used to quench cytosolic Calcein fluorescence, preserving only the mitochondrial signal. The cells were washed three times with PBS after incubation to clear away any remaining dye. Cells belonging to the PBS + L and 4TIC NPs + L groups were subjected to a 808 nm laser

irradiation at 1 W/cm² power density for 10 minutes. Calcein fluorescence intensity was captured using a fluorescence microscope. A decrease in mitochondrial fluorescence indicates the opening of the mPTP, as increased membrane permeability leads to the leakage of Calcein from the mitochondria.

Biological experiment *in vivo*

The animal experiments were approved by the Ethics Committee for Experimental Animal of The First Affiliated Hospital of Hunan Normal University (No. 2024-146).

In this study, six-week-old female C57BL/6 mice were used. each receiving a subcutaneous injection of one million tumor cells. The mice were randomly allocated into four groups once the tumor volume hit around 100 mm³ (n = 5 per group): PBS, PBS + L, 4TIC nanoparticles, and 4TIC nanoparticles + L. A total of 100 μL of PBS or 4TIC nanoparticle solution (20 μM) was injected directly into the tumor location. Here, "L" indicates laser irradiation. Mice in the PBS + L and 4TIC NPs + L groups received 808 nm laser irradiation at a power density of 1.0 W/cm² for 10 minutes. The laser spot diameter was approximately 12 – 14 mm, ensuring full coverage of the tumor, resulting in a total radiant exposure of 600 J/cm² . They were euthanized a week after the treatment.

Throughout the treatment phase, the weight of each mouse was measured with a scale, and tumor dimensions were measured with a caliper to determine tumor volume. Additionally, to evaluate survival rates, C57BL/6 mice with tumors were randomly divided into four treatment groups following the same treatment protocol, with five

mice in each group.

Infrared thermal imaging of mouse tumor

The PBS + L and 4TIC NPs + L groups of mice were subjected to a 808 nm laser with a power density of 1 W/cm² for a duration of 10 min. A thermal imaging camera was employed to take pictures and track temperature variations at the tumor location in mice with tumors during irradiation.

***In vivo* fluorescence imaging**

Following intratumoral injection of 4TIC NPs, the mice were imaged using a near-infrared (NIR) fluorescence imaging system to visualize the distribution of the nanoparticles at the tumor site.

External Laboratory Testing

Blood samples from the mice were analyzed using blood biochemistry, complete blood count (CBC), and cytokine assays. Major organs and tumors were collected, sectioned, and subjected to histological analysis.

Statistical analysis

Quantitative data are presented as the mean ± standard deviation (SD), unless otherwise indicated. Statistical analyses were performed using GraphPad Prism and R software. For in vivo experiments, each mouse was considered one independent biological replicate. Repeated measurements obtained from the same mouse over time were not treated as independent observations. Longitudinal tumor-volume and body-weight data were analyzed using a linear mixed-effects model to account for repeated measurements from the same animals. Treatment group, time, and the group × time interaction were included as fixed effects, and individual mouse ID was included as a

random effect. The group × time interaction was used to evaluate whether the temporal trajectories differed among treatment groups. Survival data were analyzed using Kaplan-Meier survival curves and compared using the log-rank test. Mice alive at the end of the 60-day observation period were treated as censored observations.

For each group, ⩾5 random fields of view were captured from at least 3 independent biological replicates (for cell experiments) or ⩾3 sections/sample (for tissue staining) captured per replicate. All image acquisition and quantitative analyses were performed in a blinded manner. ImageJ was used with a fixed threshold to segment positive signals, and fluorescence intensity or area percentage was calculated. Endpoint comparisons among multiple independent groups were performed using one-way ANOVA followed by Tukey's multiple-comparison test. Exact P values were provided where applicable. A value of $P < 0.05$ was considered statistically significant. Asterisks indicate *$P < 0.05$, **$P < 0.01$, and ***$P < 0.001$.

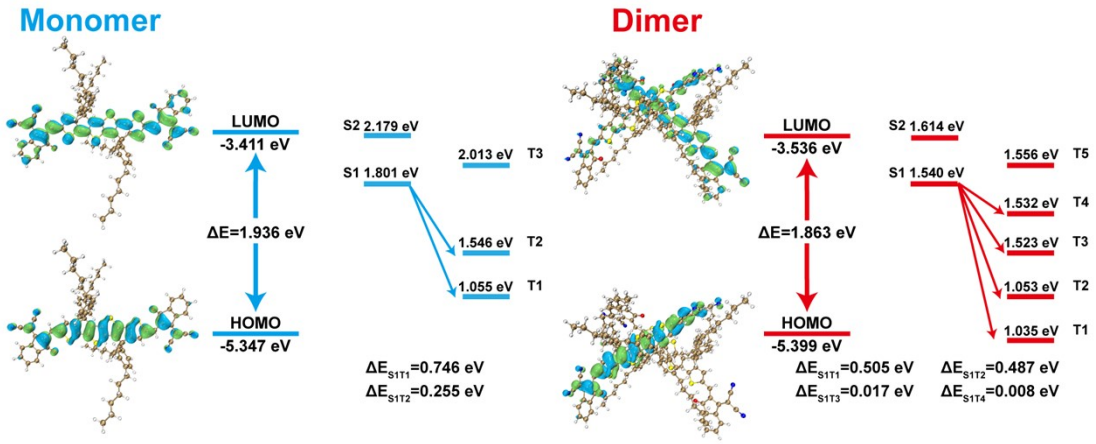

Figure S1. Diagram showing calculated frontier molecular orbital of monomeric and dimeric 4TIC NPs. Calculated energy levels of the singlet and triplet excited states of monomeric and dimeric 4TIC NPs. $\Delta E = E_{LUMO} - E_{HOMO}$.

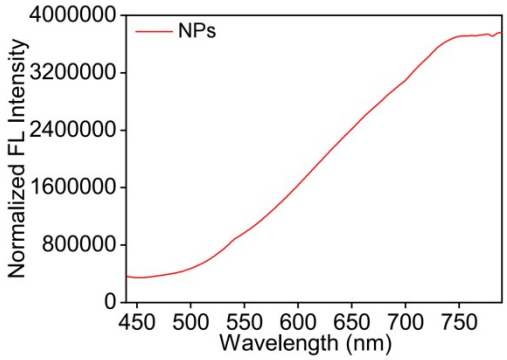

Figure S2. Fluorescence excitation spectra of 4TIC nanoparticles.

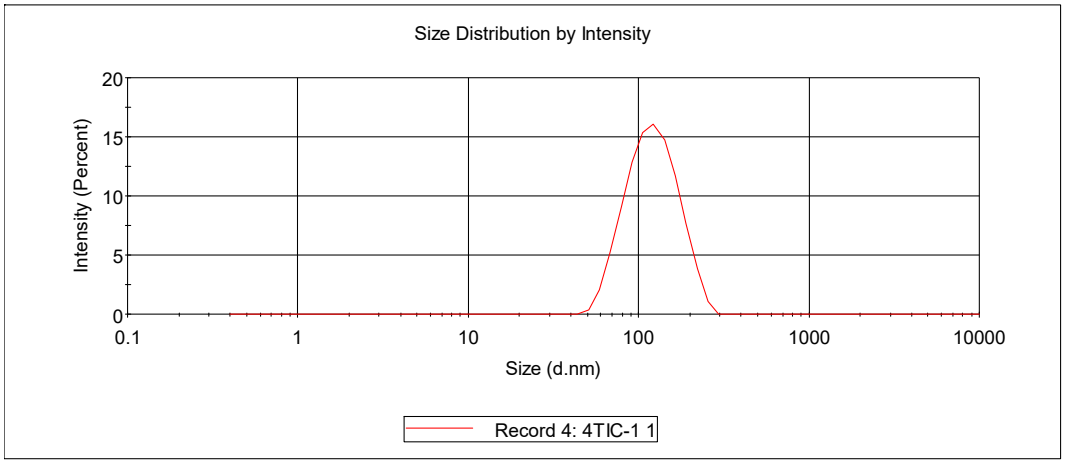

Figure S3. The DLS particle size distribution curve of NPs.

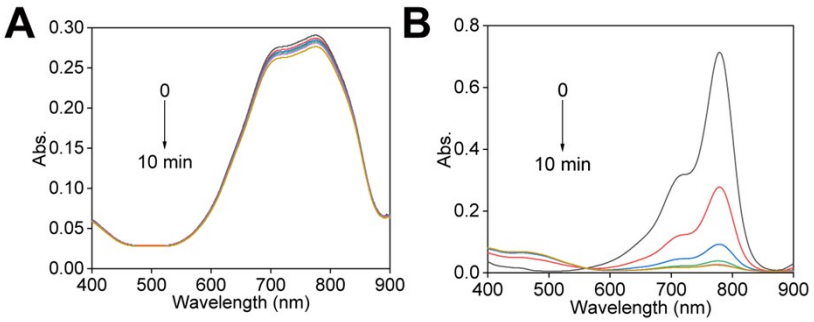

Figure S4. The change in the UV-Vis absorption spectrum of 4TIC NPs (A) and ICG (B) under 808 nm laser irradiation at 0.5 W/cm² for 10 minutes.

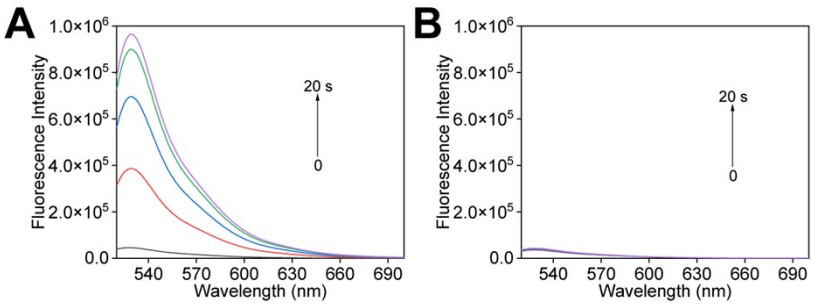

Figure S5. Fluorescence spectral variation of SOSG with (A) and without (B) of 5 μM 4TIC NPs after being exposed to 808nm laser irradiation.

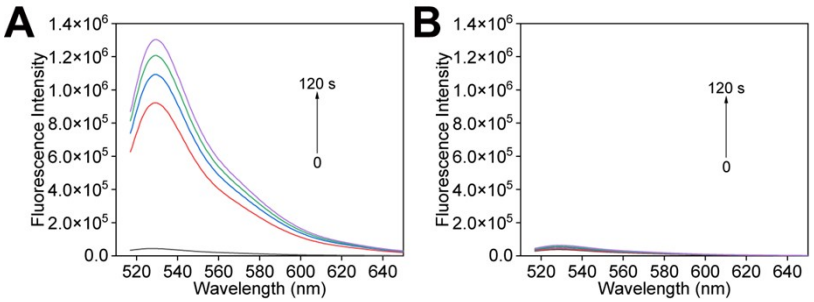

Figure S6. Fluorescence spectral variation of DHR123 with (A) and without (B) of 5 μM 4TIC NPs after being exposed to 808 nm laser irradiation.

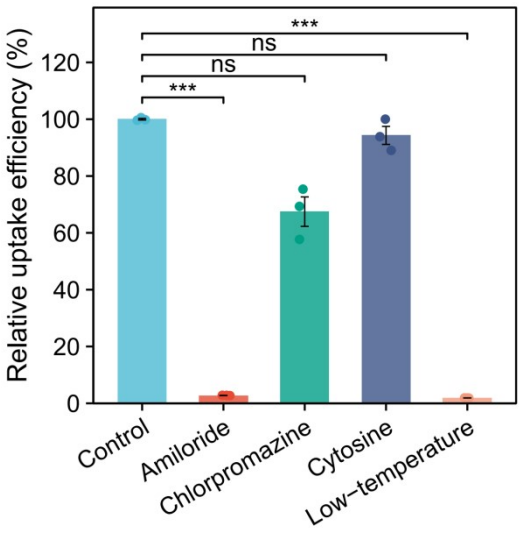

Figure S7. Flow cytometric analysis of the relative fluorescence intensity was performed on cells after treatment with various inhibitors. The data are shown as the mean ± SD, as calculated using one-way ANOVA. ***$p < 0.001$, and ns = no significance.

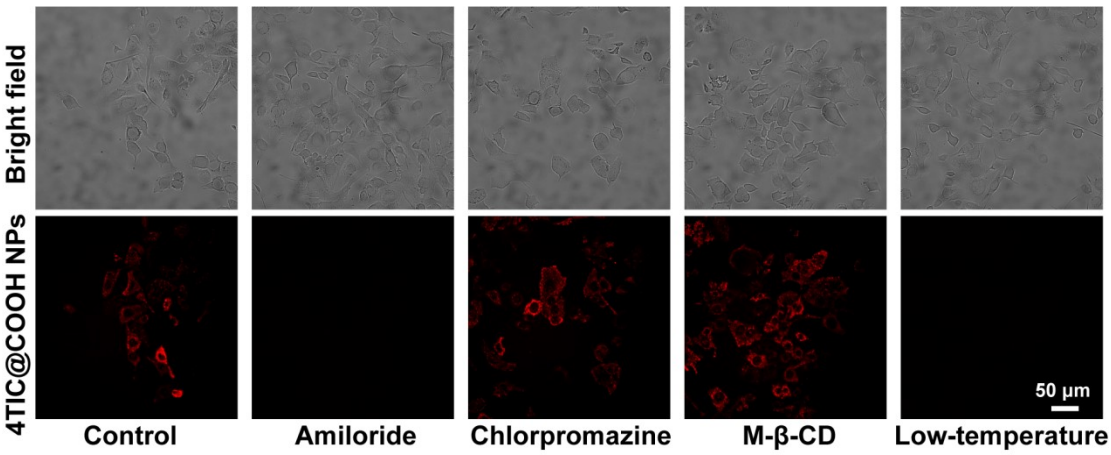

Figure S8. Cellular Uptake of 4TIC@COOH NPs by MC38 Cells following treatment with various Inhibitors.

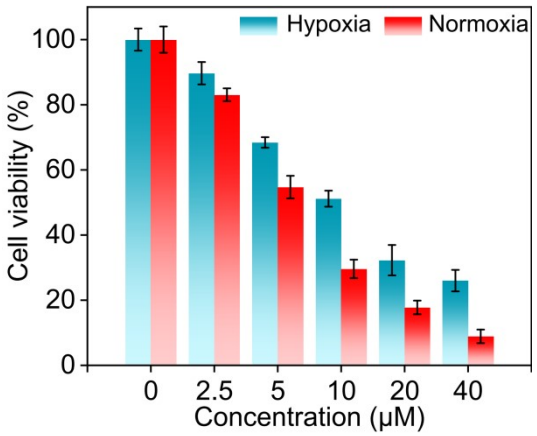

Figure S9. The NPs concentration-dependent viability of cells incubated with NPs under hypoxic and normoxic conditions.

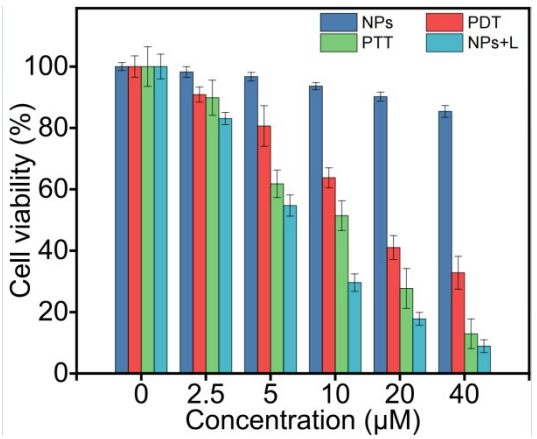

Figure S10. Quantitative detection of MC38 cells viability following PDT, PTT and simultaneous PDT/PTT.

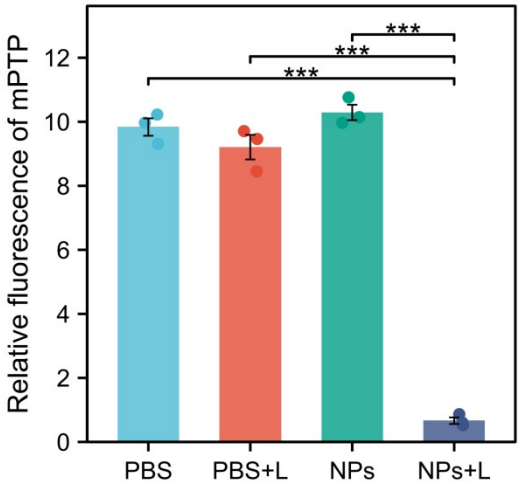

Figure S11. Statistical graph of mPTP opening in MC38 cells. The data are shown as the mean ± SD, as calculated using one-way ANOVA. ***p < 0.001.

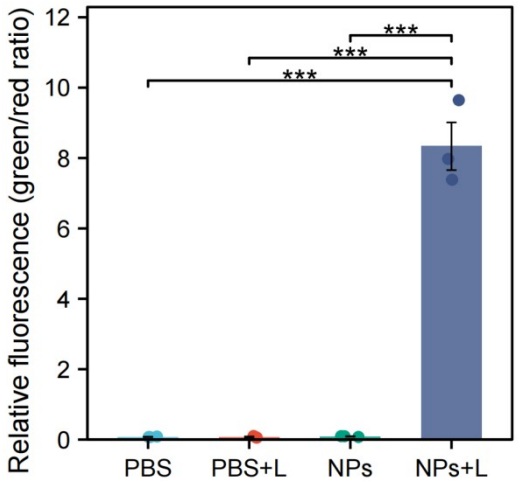

Figure S12. Statistical results of mitochondrial membrane potential (MMP) in MC38 cells after different treatments. The data are shown as the mean ± SD, as calculated using one-way ANOVA. ***p < 0.001.

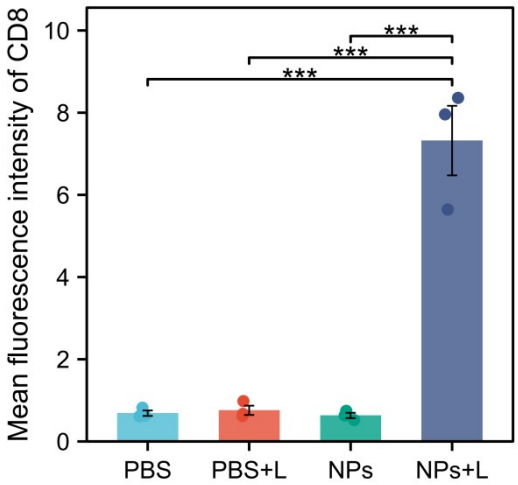

Figure S13. Quantification of intratumoral $CD8^+$ T cell infiltration across different groups. The data are shown as the mean ± SD, as calculated using one-way ANOVA. ***p < 0.001.

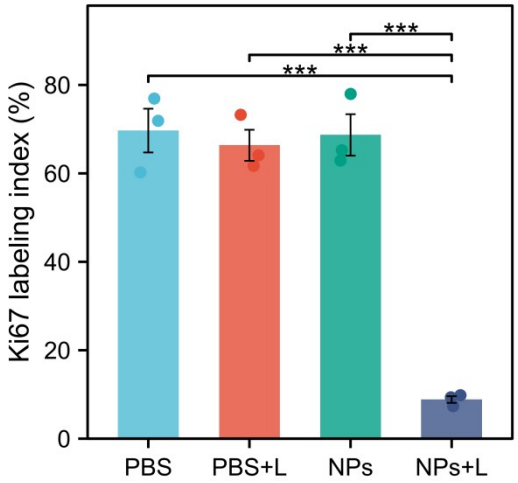

Figure S14. Quantitative analysis of Ki67 immunohistochemistry in tumor tissues. The data are shown as the mean ± SD, as calculated using one-way ANOVA. ***p < 0.001.

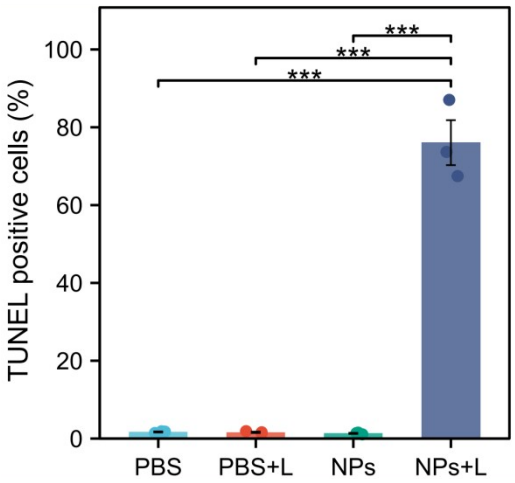

Figure S15. Quantitative analysis of TUNEL staining in tumor tissues. The data are shown as the mean ± SD, as calculated using one-way ANOVA. ***p < 0.001.

Table S1. Comparison of characteristics between 4TIC NPs and nanoplatforms.

	Singlet oxygen	Superoxide anion	Hydroxyl radical	Photothermal conversion efficiency	Immune activation	Absorption peak (nm)	Fluorescence peak (nm)	Serial number of reference

4TIC NPs	√	√	/	32.7%	√	776	850	This work
BOD-D	√	/	/	15.75%	/	635	655	[1]
FLG/ZnPc	√	/	√	14.6%	/	672	/	[2]
BDP-6@F127 NPs	√	/	/	48.46%	√	772	/	[3]
PAFH	√	/	/	40.491%	/	500-810	/	[4]

References

[1]. Sun L, Wu H, Zhang Z, Wu K, Sun J, Dong X, Dong C, Zhao C, Gu X, Qu D. A Smart Visualized Phototherapy Switch: From NIR-I Imaging-Guided Photodynamic Therapy to NIR-II-Guided Photothermal Therapy for Enhanced Cascade Tumor Photoablation. Aggregate. 2025;e70007.

[2]. Qi Y, Lv S, Xie C, Du S, Yao J. Dual-phase nanoscissors disrupt vasculature-breast cancer stem cell crosstalk for breast cancer treatment. J Control Release. 2025;377:781-793.

[3]. Peng Y, Hu C, Zhang L, Dong F, Li R, Liang H, Dai H, Jang WJ, Cheng H, Zhou L, Wang Y, Yoon J. Harnessing Dual Phototherapy and Immune Activation for Cancer Treatment: The Development and Application of BODIPY@F127 Nanoparticles. Adv Healthc Mater. 2024;13:e2401981.

[4]. Yin Y, Wong KH, Wen L, Chen M. Active Iron-Drug Nanocomplexes Improve Photodynamic and Photothermal Cancer Therapy by Mitigating Tumor Hypoxia and Counteracting Tumor Heat Resistance. Adv Healthc Mater. 2025;e2404485.